2017

Dynamics and Clustering in Locust Hopper Bands

Jialun Zhang
Harvey Mudd College

Recommended Citation

Dynamics and Clustering in Locust Hopper Bands

Jialun (Gavin) Zhang

Andrew Bernoff, Advisor

Chad Topaz, Reader

HARVEY MUDD COLLEGE

Department of Mathematics

May, 2017

Contents

List of Figures

List of Tables

Chapter 1

Introduction

In recent years, technological advances in animal tracking have renewed interests in collective animal behavior, and in particular, locust swarms. These swarms pose a major threat to agriculture in northern Africa, the Middle East, and other regions. In their early life stages, locusts move in hopper bands, which are huge aggregations traveling on the ground. Our main goal is to understand the underlying mechanisms for the emergence and organization of these bands. We construct a mathematical model that reflects experimental observations of individuals' behavior [1] and study the macroscopic emergent behavior of the group through numerical simulation.

   This work is organized as follows. In Chapter 2, we present a literature review of articles that provide the biological background on which our model is built. Key information from each article that might be relevant to the model is outlined in bullet points. In Chapter 3, we introduce the mathematical model of locust motion on the infinite 2-dimensional plane. The equations of motion are given, and we also present our methods of estimating the relevant parameters in the model. The results of the estimations are summarized in Table 3.1. In Chapter 4 we present some simulation results in Matlab. In particular, we give examples of parameters at which a phenomenon known as fingering occurs. We also present results for a few extreme cases where the parameters are very much exaggerated. In Chapter 5, we develop metrics for characterizing the behavior of the swarm in our simulations. We also build a clustering algorithm to identify the fingers in the swarm. In Chapter 6, a new model is presented for locust motion on the periodic rectangular domain, and an addition equation is added to account for attraction between locusts. In Chapter 7, a PDE model on a periodic domain is derived. The stationary solutions are found under certain assumptions, and the stability

of these solutions are studied. Finally in Chapter 8, we present a summary of the work that has been done and some possible future directions.

Chapter 2

Literature Review

In this section we give an overview of some of the biological literature that is relevant to our research. While not all of the information are used in the model, the information in this chapter could provide useful directions for future work.

2.1 Desert Locust Guidelines, Symmons and Cressman (2001)

This paper gives basic information on the biology and behavior of the Desert Locust. We summarize the some of the useful information.

2.1.1 Biology of Locusts

Adult locusts can form swarms which may contain thousands of millions of individuals and which behave as a unit. The non-flying nymphal or hopper stage can form bands, where a band is defined as a cohesive mass of hoppers that persists and moves as a unit. Locusts have two different states called phases: solitarious and gregarious. When locusts are present at low densities, the individuals are solitarious. As locust numbers increase, they cluster into dense groups and they become gregarious. Being touched by others, especially on the outer surfaces of the hind femora (thighs), results in locusts being attracted rather than repelled by others, and so they form groups.

2.1.2   Hopper Groups and Bands

As hopper numbers increase in certain habitats, their behavior changes - they accumulate and become concentrated. This can happen when hoppers are sheltering in vegetation, during basking, feeding and roosting, and when they are moving on the ground. Grouping often occurs in open habitats that are less uniform, where there are patches of relatively dense vegetation separated by large areas of bare soil. When low densities of solitary hoppers are present in uniform habitats consisting of low plants and bare soil of in habitats of uniform dense vegetation, groups are less likely to form. Shortly after hatching, hoppers form small dense black patches. These patches may cover no more than a few tens of square centimeters, but contain several thousand insects per square meter. During warm and sunny days, hopper bands follow a pattern of behaviour alternating between roosting and marching throughout the day. On overcast days, bands usually do not move very far. Maximum densities of bands on the ground range from over 30000 hoppers per square meter for first instars to just over 1000 per square meter for the fifth instar. However, average densities are much lower. For late instar bands, density is probably between 50 and 100 hoppers per square meter. The rate of band movement varies with temperature, vegetation cover and even with the size and coherence of the band. Bands usually maintain a constant heading during a day; even a major obstruction is not always sufficient to change its path. The heading is often, but not always, downwind. At midday, bands usually roost in the vegetation.

2.1.3   Effects of Vegetation

On *bare soil*, hoppers usually spend most of their time moving over the bare ground, alternating with resting and basking (facing of parallel to the sun). In a habitat where the vegetation is *evenly distributed and consists of small, low plants with only small areas of bare ground in between*, hopper behavior is similar to that in bare soil but is modified by movements in and out of the vegetation. Hopper movement is reduced under cloudy skies or in the early hours of clear cold mornings. *Non-uniform vegetation cover of mixed plants*. Hoppers spend very little time on the ground and most of the time in the vegetation in habitats consisting of large, dense, low plants where the plants are separated by large areas of bare ground. They mainly move up and down within the vegetation during the day. During overcast conditions, hoppers spend nearly all the time in vegetation. *Non-uniform vegetation cover of taller*

plants. Hoppers move up and down within the vegetation and towards the east and west in habitats where there are relatively tall plants with an open structure.

2.2   Individual Pause-and-Go Motion Is Instrumental to the Formation and Maintenance of Swarms of Marching Locust Nymphs, Ariel et al. (2014)

This paper studies the collective behavior of locust swarms. It provides new insights into the mechanisms responsible for coordinated locust motion.

The experiments suggest that collective movement is highly dependent on the density of animals in the group, and is mediated by social pairwise interactions such as avoidance, alignment, and attraction. It was also shown that groups can switch direction *without* external perturbation. Pause duration is associated with a high probability of turning. This result suggests that pauses relate to instances in which individuals make a choice on direction. Assisted by simple models, the paper shows that intermittent motions have a pivotal role in the development of order and disorder in the system. Nymphs rarely change direction while walking. Experimental observation: desert locust nymphs present a walking pattern of intermittently switching between walking and pausing. The paper looked for mechanisms involved in the decision of a standing locust to initiate walking. The most consistent factor was found to be an increase in the average number of walking locusts in the proximity of the standing locust. Further investigation reveals that in many cases (54%), walk initiation was preceded by the standing locust being bumped by another locust. However, this phenomenon might as well be a result of the physical constraint of the experimental arena, since bumping is rarely seen in the wild marching band. The paper finds (using experiments) that on average, right before a locust starts moving, it senses a decrease in the number of moving individuals in front of it, or an increase in the number of moving individuals behind it.

2.2.1   The Role of Visual Cues in Collective Motion

The paper presents some neurophysiological evidence for the role of visual cues in the collective motion of locusts. The experiments uses two kinds of visual cues: objects receding in the frontal visual field and objects

approaching in the rear visual field. I summarize some of the main results below:

The locust responds to visual cues from *all directions*. Objects *approaching* the locust generates stronger neural responses. Multiple visual cues generates stronger responses than single visual cues. This means that two locusts approaching will elicit stronger neural response than just one locust approaching.

2.3 Intermittent Motion in Desert Locusts: Behavioural Complexity in Simple Environments, Bazazi et al. (2012)

This paper looks at the motion of *individual* locusts in simple environments. The locust is placed in an empty arena, so the influence of external factors (such as environmental cues or other locusts) is minimized. The paper identifies some of the statistical properties of the pause-and-go movement of the single locust. Our quantification of locusts' turning behavior both within pauses and within moves demonstrates that a change in direction is more likely to be found in a pause than in a move. Therefore, we can consider moves as displacements without change in direction, and pauses as opportunities for turns. The duration of a pause influences the probability that a locust changes direction after the pause. The data show that the mean probability for a locust to turn within a pause increases with the pause length. However, the probability reaches a plateau near 6s.

2.4 Inherent Noise can Facilitate Coherence in Collective Swarm Motion, Yates et al. (2009)

This paper argues that noise in locust motion can help individual locusts align with the rest of the swarm. The locusts appear to increase the randomness in their motion in response to loss of alignment with the group. The authors identify *the mean switching time* as an important parameter for quantifying collective behavior, and much of the mathematical derivation in the paper involve the diffusion process and the Fokker-Planck equation. I summarize some of the conclusions of the paper below.

The paper established that the mean switching time increases exponentially with the number of locusts. As locust density increases, the turning rate

of the group rapidly increases. This observation has important implications: at high densities, it becomes increasingly difficult to influence a group's direction. The paper used the systematic Fokker-Planck equation coefficient estimation approach on experimental data. The results indicate that the individuals move more randomly in locust groups with low alignment. This appears to enable the group to find (an remain in) a highly aligned state more easily. The paper suggests that recent finding about cannibalistic interactions could provide a rationalization for for the observation of apparently increased individual randomness in response to a loss of alignment at the group level: given the risk of exposing the rear of the abdomen to oncoming insects, there may be selection pressure on an individual to minimize the time spent in the disordered phase. A longer inter switch time might also be selected for in an evolutionary scenario since it allows the locusts to remain in a coherent group for longer periods, potentially increasing harvesting efficiency and reducing predation.

2.5   From Disorder to Order in Marching Locusts, Buhl et al. (2006)

Using a SPP (self-propelled particle) model of locust swarms, this paper identifies a critical density where a rapid transition occurs from disordered to ordered movement. The paper also demonstrates dynamic instability in motion at densities typical of locusts in the field, in which groups can switch direction without external perturbation, potentially facilitating the rapid transfer of directional information.

The authors of the paper defined the orientation χ of a locust as the smallest angle between one line drawn between the locust's two consecutive positions and a second line drawn from the center of the arena to the locust's first position. This relationship can be described as $\chi = \arcsin\left[\sin(\theta - \alpha)\right]$, where α is the angle of the direction of movement and θ is the angle with the center of the arena. For each camera image, the instantaneous alignment Φ^t is defined average of the orientation for all moving locusts, normalized as

$$\Phi^t = \frac{2}{m\pi} \sum_{i=1}^{m} \chi_i^t$$

where m is the total number of *moving* locusts, and i is the ith locust. Thus, values of alignment close to the extreme values of 1 and -1 indicate the

alignment of all locusts in the same direction, whereas values close to zero indicate an absence of any collective alignment.

A central prediction of the model developed by Vicsek and collaborators is that as the density of animals in the group increases, a rapid transition occurs from disordered movement of individuals within the group to highly aligned collective motion. It has been shown in laboratory that marching begins only at high locust density. The average density of marching locust bands in the field is 50 locusts per square meter, with a typical range of 20 to 120 locusts per square meter. Coordinated marching behavior depended strongly on locust density. At low densities (5.3 to 17.2 locusts/m^2), there was a low incidence of alignment among individuals. Intermediate densities (24.6 to 61.5 locusts/m^2) were characterized by long periods of collective rotational motion with rapid spontaneous changes in direction. At densities above 73.8, spontaneous changes in direction did not occur within the timescale of the observation, and the locusts quickly adopted a common and persistent rotational direction. Both the experiments and the SPP model exhibits dynamic instability, in which changes in direction are sudden and spontaneous, rapidly spreading through the entire group. The experiments show that these changes can be independent of external conditions and are likely to be an inherent property of moving groups. The data and model also suggest that predicting the motion of very high densities of locusts is easier than predicting that of intermediate densities. The small number of directional changes at high densities, observed during 8 hours of our experiments, was similar to the field observation of "gregarious inertia" that lasts for days.

2.6 Collective Motion and Cannibalism in Locust Migratory Bands, Bazazi et al. (2008)

This paper provides evidence that locust collective behavior is strongly influenced by cannibalistic interactions. An individual locust's decision to move forward is the result of two cues: tactile stimulation and the rear visual field.

Reduction of individuals' capacity to detect the approach of others from behind through abdominal denervation decreases their probability to starting moving, reduces the percentage of moving individuals in groups, and significantly increases cannibalism. The authors also tested the prediction that cannibalism serves as a general mechanism for the transition from

relatively disordered and benign aggregations to highly coordinated and mobile bands which are responsible for the devastating impact of marching locusts. Removal of the sensation from the abdomen did not inherently influence individual motion, but reduction of the sensation of individuals approaching from behind had a very strong negative influence on marching behavior in groups; the mean proportion of moving locusts and their mean speed when moving were significantly lower in abdomen-denervated groups. These results demonstrate that sensation of contact of others from behind plays an important role in determining the extent to which locusts will move, as well as the resulting degree of coordinated movement among individuals in marching bands. Relative to contact from conspecifics approaching in other directions, contact from behind resulted in the highest probability (0.65) of movement among the sham-operated insects. Visual stimuli are also potentially important in marching coordination. Groups of individuals with no restriction of visual input (control) showed significantly higher levels of marching than those with a complete restriction of visual input (totally blind). The study suggests that cannibalistic interactions among individuals, and the threat of attack by those approaching from behind, is a principal factor in the onset of collective movement among locusts. Individuals increase the propensity of others to march as they approach toward, or contact, their abdomen.

2.7   Group Structure in Locust Migratory Bands, Buhl et al. (2011)

Using data collected from actual recording of locust bands, this paper captures the fundamental features of locust bands in the field.

The density profiles showed an extremely inhomogeneous structure, with a single peak at the front, followed by a sharp, exponential decay, as shown by the linear trend on a semi-logarithmic representation. Qualitative descriptions and aerial photographs of large bands indicate a very similar marked concentration of locusts at the front (the larger the bands, the higher the peak densities and the deeper the fronts) that vanishes rapidly behind it. The density of locusts ranged roughly from 50 locusts/m^2 on average to 1200 locusts/m^2 in the front. Densities above roughly 50 mâĹŠ2 showed consistently high levels of polarisation, whereas those below showed large variation in polarisation, suggesting a weaker alignment of locusts. By testing the distribution of polarisation of pairs separated by increasing distance, the

authors determined that this distribution ceased to be significantly different from uniform beyond 13.45 cm apart. The alignment between individuals that determines band cohesion and movement occurs within a distance of only 13.5 cm. Bands comprise an extremely dense front followed by an exponential decay of density, with a consequent loss of cohesion towards the back.

Chapter 3

A Mathematical Model of Locust Swarms

Our goal in this section is to develop a continuous version of the Alignment and Intermittent Motion (AIM) model of locust swarms developed in the works of Jones, Devore and Schein (Jones 2016).

3.1 Equations of Motion

We introduce a continuum version of the Alignment-Intermittent Motion (AIM) model of locust swarms. Let $x_i \in \mathbb{R}^2$ to denote the current position of a locust. The unit vector $\hat{u}_i$ represents the direction that the locust is currently facing, and in polar coordinates we can write

$$\hat{u}_i = (\cos \theta_i, \sin \theta_i). \tag{3.1}$$

Each locust has two states, moving or stationary. This is represented by the variable s_i, where $s_i = 0$ when stationary and $s_i = 1$ when moving. Suppose that all locusts move with constant velocity v_0, then the instantaneous velocity at some position x_i is given by the equation

$$\frac{dx_i}{dt} = v_0 s_i \hat{u}_i. \tag{3.2}$$

Each locust updates its orientation by trying to align itself with the locusts nearby. To diminish the influence of locusts that are too far away, we introduce a weight function $g(z)$. We model the process of alignment using

the equation

$$\frac{d\theta_i}{dt} = -\sum_{j=1, j\neq i}^{n} g(z_{ij}) \sin(\theta_i - \theta_j) + W \tag{3.3}$$

where W is Gaussian random noise, $z_{ij} = \|x_i - x_j\|$, and θ_i is the orientation (in radians) of the current locust. Note that the deterministic part of this model is of Kuramoto type, which was described in Strogatz (2000). For the weighting function $g(z)$, we take

$$g(z) = c_a \left(1 - \frac{z}{\ell_a}\right), \tag{3.4}$$

for $z \leq \ell_a$ and zero otherwise. Here, c_a is a weighting parameter measuring the maximal influence of neighbors and ℓ_a is a length scale of alignment influence.

3.2   Transition Probabilities

The method for calculating the transition probabilities in this section are described in Segel and Edelstein-Keshet (2013). In equation (3.2), the variable s_i changes from 0 to 1 and vice-versa in a Markov process. At the population level, this process can be modeled as a differential equation. Suppose A is the population of locusts that are stationary and B is the population that are moving. The rate constant k_1 is defined such that for sufficiently small Δt, $k_1 \Delta t$ is the probability that a particle shifts from stationary to moving in the time interval Δt. Similarly, k_2 is defined such that $k_2 \Delta t$ is the probability that a particle shifts from moving to stationary in the time interval Δt. Therefore, the expected change in the number of stationary locusts in the time interval $(t, t + \Delta t)$ is

$$A(t + \Delta t) - A(t) = -A(t) \cdot (k_1 \Delta t) + B(t) \cdot (k_2 \Delta t). \tag{3.5}$$

Dividing by Δt and taking the limit as $\Delta t \to 0$, equation (3.5) becomes

$$\frac{dA}{dt} = -k_1 A + k_2 B. \tag{3.6}$$

Similarly, the corresponding equation for B is

$$\frac{dB}{dt} = k_1 A - k_2 B. \tag{3.7}$$

Using this model, we claim that in some time interval $(t, t + \Delta t)$ (where unlike before, Δt is arbitrary), the probability that a particle changes from stationary to moving is given by

$$P_{sg} = \frac{k_1}{k_1 + k_2} \left(1 - e^{-(k_1 + k_2)\Delta t}\right). \tag{3.8}$$

Similarly, the probability that a particle changes from moving to stationary in the time interval $(t, t + \Delta t)$ is given by

$$P_{gs} = \frac{k_2}{k_1 + k_2} \left(1 - e^{-(k_1 + k_2)\Delta t}\right). \tag{3.9}$$

These expressions come from solving the linear differential equations above. Notice that when Δt is small, we find that $P_{sg} = k_1 \Delta t$ and $P_{gs} = k_2 \Delta t$, which is consistent with how we defined k_1 and k_2.

Now, to determine P_{sg} and P_{gs}, we need to estimate k_1 and k_2. To do this, we define a blocking score β_i for each particle, which is a metric for measuring how much a locust is obstructed by its neighbors. We claim that the larger the blocking score is, the less likely a locust is to change from stationary to moving and the more likely it is to change from moving to stationary. Therefore, we can write

$$k_1 = \kappa_1 e^{-a_1 \beta} \quad k_2 = \kappa_2 e^{a_2 \beta},$$

where κ_1, κ_2 and a_1, a_2 are constants.

The blocking score β is determined from the configuration of the locust swarm. For a locust at position x_i and its neighbor at x_j, we can define the relative distance $z_{ij} = |x_i - x_j|$ and the relative angle, ϕ_{ij}, satisfying

$$\cos \phi_{ij} = (x_j - x_i) \cdot \hat{u}_i / z_{ij}. \tag{3.10}$$

Then the blocking score for the locust at x_i is

$$\beta_i = \sum_{\substack{j=1 \\ j \neq i}}^{n} f(z_{ij}, \phi_{ij}) \tag{3.11}$$

where $f(z, \phi)$ is a weight function given as

$$f(z, \phi) = \left(1 - \frac{z}{\ell_b}\right) \cos \phi, \tag{3.12}$$

for $z \leq \ell_b$ and zero otherwise. Here ℓ_b is the length scale of blocking influence. We expect that neighbors in front of the current locust contribute to it being blocked (and hence being more likely to be in a stopped state) whereas neighbors in back of the locust contribute the likelihood to move. These effects are reflected in the term $\cos \phi$.

3.3 Discretization of the Model

To simulate the behavior of swarms, we have to discretize our continuous model. Consider the system at the times $t_1, t_2 \ldots$ where $\Delta t = t_{n+1} - t_n$ is a constant. The difference equation for updating the position is then

$$x_i(t_{n+1}) = x_i(t_n) + (v_0 \Delta t) \cdot s_i \cdot \hat{u}_i. \tag{3.13}$$

Similarly, we update the orientation θ_i (equivalently, $\hat{u}_i$) using

$$\theta_i(t_{n+1}) = \theta_i(t_n) - \left(\sum_{j=1, j \neq i}^{n} g(z_{ij}) \sin (\theta_i(t_n) - \theta_j(t_n)) \right) \Delta t + Q(\Delta t). \tag{3.14}$$

Here $Q(\Delta t) = \xi \sqrt{D \Delta t}$ is the displacement due to the Gaussian random noise W over time Δt. Note ξ is a Gaussian random variable with mean 0 and variance 1 and D is a diffusion constant with units $(\text{radians})^2/s$.

In each step, we also have

$$P(s_i(t_{n+1})|s_j(t_n)) = \mathcal{S} \tag{3.15}$$

where $\mathcal{S}$ is the transition matrix

$$\mathcal{S} = \begin{pmatrix} 1 - P_{sg} & P_{sg} \\ P_{gs} & 1 - P_{gs} \end{pmatrix} \tag{3.16}$$

and the variables P_{sg} and P_{gs} are determined above.

3.4 Parameters of the Model

In this section we summarize all the parameters used in the model, which are given in the Table 3.1. The parameters are estimated from the biological literature.

- To estimate the constants κ_1 and κ_2, we used the results of Ariel et al. (2014), where in their Figure 1 (C&D), the distribution of walk times and pause times were plotted. The authors claim that the distribution of of pause times shows a power-law decay while the distribution of walking times is well-approximated by an exponential distribution. This means that $k_1 \approx 0.16$. However, if we also try to fit an exponential distribution to the pause times, we find that $k_2 \approx 0.1$. This gives us a range for both k_1 and k_2.

- The alignment length scale ℓ_a is the radius in which the influence of other locusts is significant for alignment. In both Ariel et al. (2014) and Buhl et al. (2011), this distance was found to be around 13 cm.

- We assumed that ℓ_b, the blocking length scale, is approximately equal to the body length of locust, which is well-documented in the biological literature.

- The typical density of the swarms, ρ, ranges from 50-1200 locusts per m^2. This is documented in Buhl et al. (2011).

- To approximate the block score β, we compute the integral

$$\beta_{\max} = \int_{-\pi/2}^{\pi/2} \int_0^{\ell_a} \rho z \left(1 - \frac{z}{\ell_a}\right) \cos\phi \, dz d\phi = \frac{\ell_a^2 \rho}{3}.$$

Thus the range of ρ and ℓ_a gives us an estimation of the range of β.

- The velocity of individual locusts v_0, is documented in the biological literature, and can be found in Bazazi et al. (2008).

- The angular diffusion constant D scales a Gaussian noise. This parameter is estimated to be 1 from the distribution of turning angles found in Figure S5 of Ariel et al. (2014).

- An estimation of a_1 and a_2 can be made using the data available in Figure 2 of Bazazi et al. (2008). Assuming that the block score of a single locust being contacted by another locust from behind is -1, we find that

$$\frac{k_1(\text{untouched})}{k_1(\text{touched})} = \frac{k_1 e^0}{k_1 e^{-a_1 \beta}} = e^{-a_1} = 0.8.$$

Thus we get $a_1 = 0.22$. Since a_1 and a_2 are governed by the same biological mechanisms, we also estimate that $a_1 \approx a_2$, so we estimate that $a_2 = 0.22$.

- Finally, we need an estimation for the turning rate c_a. According to Equation 3, c_a can be viewed as the turning rate of locust i that is at $\pi/2$ from locust j at the same spot. In Dyson et al. (2015), Equation 2 models the situation when two locusts come in contact with one other locust going in the other way. The transition occurs with rate r_2, which is listed in Table 1 in the paper (normalized by the number of locusts). In the case of one locust switching direction, we have $r_2 \approx 0.036 \cdot 5^2 = 0.9$. This gives us an estimation for c_a. Therefore, we set the sampling range for c_a to be $0.3 - v3$.

Parameter	Description	Sampling Range	Range of Values	References
M	total number of locusts	N/A	5000-1000000	
v_0	velocity of an individual locust	2-8 cm/s	3-4 cm/s	Bazazi et al. (2008), p2
D	angular diffusion, scales a Gaussian noise	0.03-0.3	1	
ℓ_b	Blocking length scale, currently, body length of locust	1-10 cm	1.2-7.5 cm	Nat Geo
ℓ_a	Alignment length scale, currently, sensing radius	1-15 cm	around 13 cm	Ariel et al. (2014) and Buhl et al. (2011)
κ_1	amplitudes for rate constant	0.05-0.5 s^{-1}	1 s^{-1}	
κ_1	amplitudes for rate constant	0.03-0.3 s^{-1}	1 s^{-1}	
a_1, a_2	constant in the exponent of rate constant	0.07 - 0.6	around 0.22	
c_a	a scaling constant for alignment	0.3-3 s^{-1}	1 s^{-1}	
ρ	the initial density of the locusts	0.05-0.12 locusts /cm^2	50-1200 locusts/m^2	Buhl et al. (2011)
β	block score	$1.6 \cdot 10^{-3} - 2.7$	$l_a^2 \rho/3$	

Table 3.1   Table of Parameters

Chapter 4

Simulation Results

Our simulation for both a relatively small number of locusts and a large number of locusts show that the swarms exhibit a phenomenon known as *fingering*. Initially the locusts are clumped together. The initial position and heading of a locust is chosen randomly from uniform distributions. We show some of the results in Figures 4.1-4.7. For figures 4.1 and 4.2, we have set $\kappa_1 = 0.8$ and $\kappa_2 = 0.2$. The amplitude for alignment is $c_a = 0.5$.

To investigate how the swarm is influenced by different parameters, we look at a few extreme cases. Figure 4.3 shows that resulting behaviour with we set $\kappa_1 = 1$ and $\kappa_2 = 0$, which corresponds to constant motion since the probability of stopping is 0. On the other hand, we can set $\kappa_1 = 0$ and $\kappa_2 = 1$, so that the probability from stop to go is 0. The result is not too surprising: the swarm remains stationary in their initial clump, as shown in Figure 4.4.

For all the simulations above, we have set the alignment amplitude to be $c_a = 0.5$. In Figure 4.5, we look at the case where the alignment amplitude is very large ($c_a = 10$). For the following results we set $\kappa_1 = 0.8$ and $\kappa_2 = 0.2$. We can see from the figure that when alignment is too strong, the locuts just seem to scatter outwards. Now we look at the case where alignment is very weak. We set $c_a = 0.01$, and the result is shown in Figure 4.6.

For all the previous simulations, the initial heading of the locusts were chosen randomly from a uniform distribution on $[0, 2\pi]$. In Figure 4.7, we show that result when we initialize all the locusts to be facing the positive y direction initially. In this case, the swarm initially moves slowly together in the positive y direction as a clump, but then fingers towards different directions.
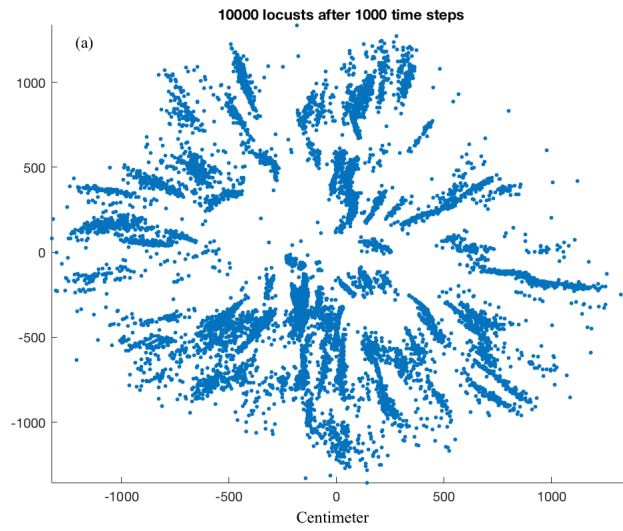
Figure 4.1 $M = 10000$, $\kappa_1 = 0.8$, $\kappa_2 = 0.2$ and $c_a = 0.5$
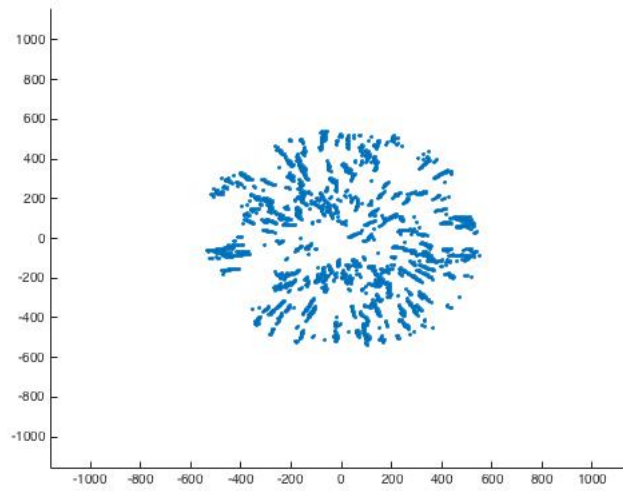
Figure 4.2 $M = 1000$, $\kappa_1 = 0.8$, $\kappa_2 = 0.2$ and $c_a = 0.5$
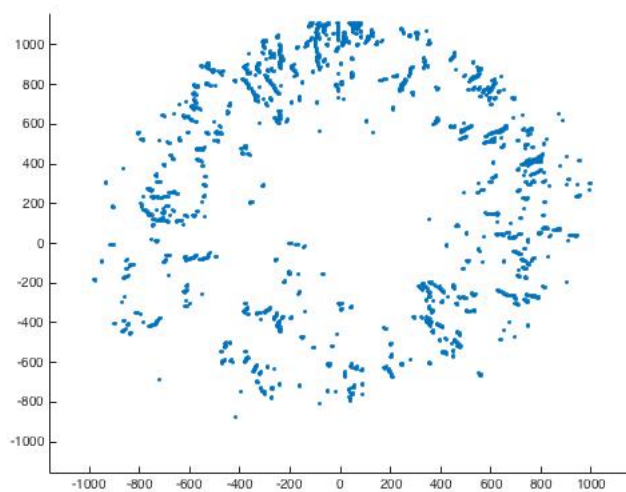
Figure 4.3 $M = 5000$, $\kappa_1 = 1$, $\kappa_2 = 0$ and $c_a = 0.5$
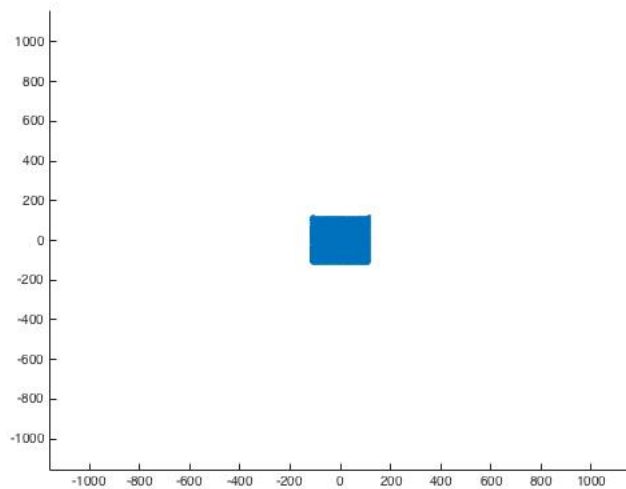
Figure 4.4 $M = 5000$, $\kappa_1 = 0$, $\kappa_2 = 1$ and $c_a = 0.5$
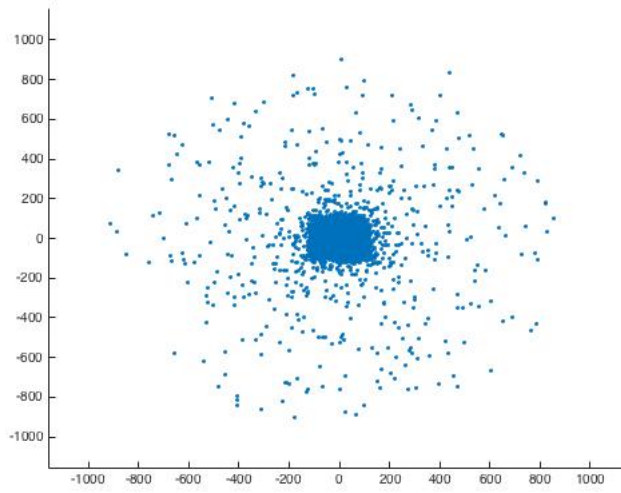
Figure 4.5 $M = 5000$, $\kappa_1 = 0.8$, $\kappa_2 = 0.2$ and $c_a = 10$
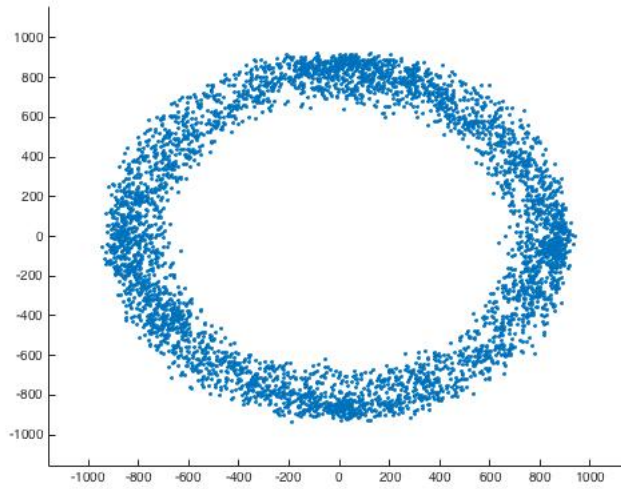
Figure 4.6 $M = 5000$, $\kappa_1 = 0.8$, $\kappa_2 = 0.2$ and $c_a = 0.01$
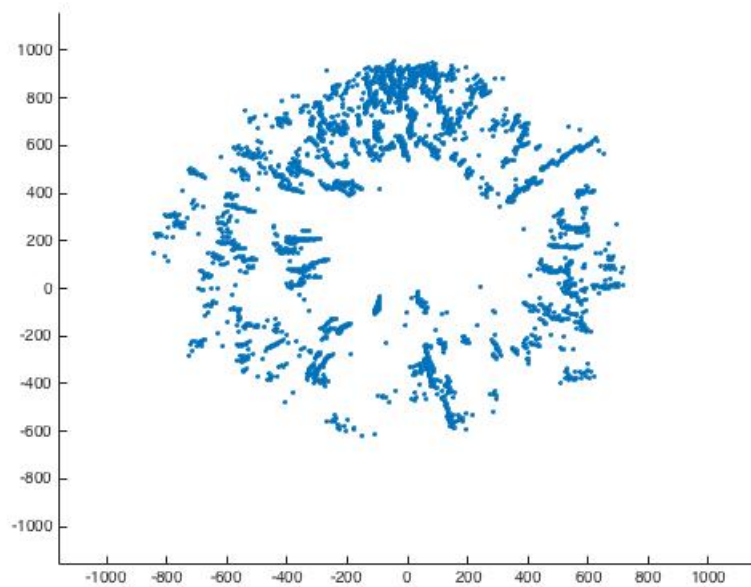
Figure 4.7   All initial heading are in the positive y direction, $M = 5000$, $\kappa_1 = 0.8$, $\kappa_2 = 0.2$ and $c_a = 0.5$

Chapter 5

Metrics for Characterizing the Geometry of the Swarm

5.1 Average Density

We would like to define an average density ρ for the whole swarm, and look at how ρ evolves as a function of time. The main difficulty here is to define a perimeter for the swarm so that we can effectively calculate the density. To do this, we use the build-in Matlab function `alphaShape`, which allows us to identify the boundary of a point cloud using an 'alpha shape' - a generalization of the convex hull. An example is shown in Figures 5.1 and 5.2. Once we have a perimeter for the swarm, we can define the density as

$$\rho(t) = \frac{M}{A(t)},$$

where M is the total number of locusts and $A(t)$ is the area of the alpha shape at the current time step.

5.2 Local Density

The local weighted density ρ_{loc}^i is defined for the i-th locust as

$$\rho_{\text{loc}}^i = \frac{1}{\pi r^2} \sum_{j \in I} (1 - \frac{z_{ij}}{\ell_a})$$

where I is the index set for all the locusts within radius ℓ_a of the i-th locust (not including itself).
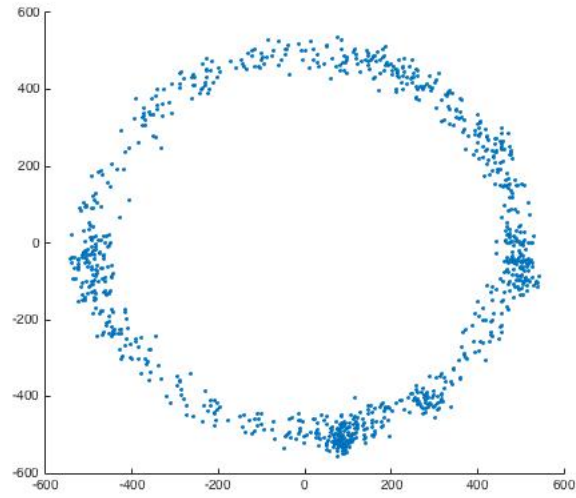
Figure 5.1   An example of a point cloud
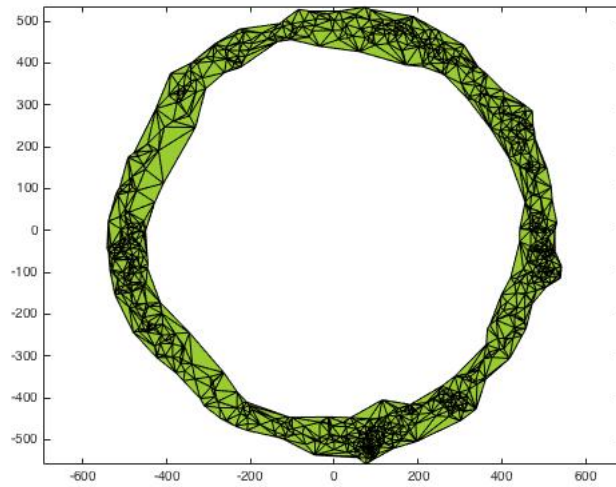
Figure 5.2   The boundary generated by Matlab

5.3   Global and Local Orientation

The global orientation is simply defined as

$$\gamma = \frac{1}{M} \sum_{j=1}^{M} \hat{u}_j,$$

where $\hat{u}_i$ is the orientation of the j-th locust and M is the total number of locusts. Similarly, the local orientation is defined for each locust as

$$\gamma_{\text{loc}}^{i} = \frac{1}{|I|} \sum_{j \in I} \hat{u}_j$$

where I is the index set for all locusts within the sensing radius ℓ_a.

5.4   Global and Local Alignment

For each individual locust, the local alignment parameter is defined as

$$\psi_{\text{loc}}^{i} = \sum_{j \in I} (\hat{u}_i \cdot \hat{u}_j) g(z_{ij}) / \sum_{j \in I} g(z_{ij}),$$

where I is the index set of all locusts within radius ℓ_a of the i-th locust (including itself). Taking the average of the local alignment parameters for every locust, we get the global alignment parameter:

$$\psi = \sum_{i=1}^{M} \psi_{\text{loc}}^{i},$$

where M is the total number of locusts.

5.5   Average Velocity for Individual Locusts

Since we assume that when locusts are moving, they travel at a constant velocity v_0, the average velocity is simply

$$\bar{v} = \alpha v_0,$$

where α is the percentage of the time that the locust is moving.
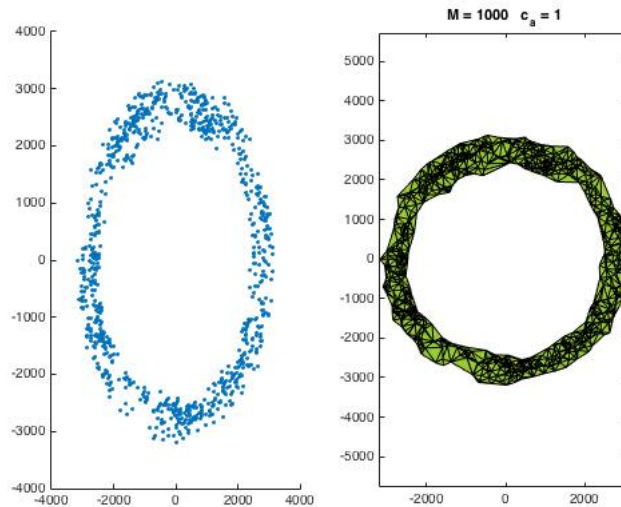
Figure 5.3   Example 1(a): Plots of the point cloud at the final time step

5.6   Area and Perimeter of the Swarm

The area of the perimeter of the swarm can be identified once we know the boundary of the swarm, which can be given by the Matlab function `alphaShape`. These two values can be useful in identifying phenomenon such as fingering.

5.7   Example 1

In the figures 5.3-5.5, we show some plots of the metrics that we have just defined for a particular swarm. For this run, we have chosen $k_1 = 0.8$, $k_2 = 0.2$, $a_1 = 1$, $a_2 = 1$ and $c_a = 1$. The total number of locusts is $M = 1000$, the initial density was set to 1, the time step was $\Delta t = 1$, and the results are shown for 2000 time steps.

5.8   Example 2

In Figures 5.6-5.8, we show the plots of some metrics for another swarm where there is no apparent fingering in the system. For this run, we have chosen $k_1 = 0.8$, $k_2 = 0.2$, $a_1 = 1$, $a_2 = 1$ and $c_a = 10$. The total number of
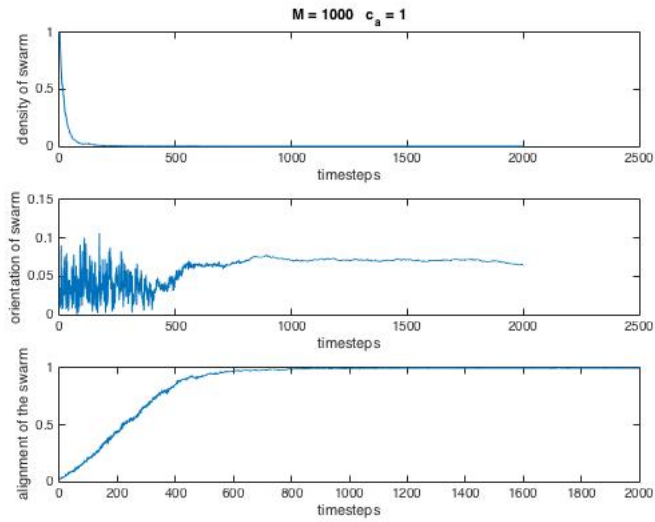
Example 2   27

Figure 5.4   Example 1: Plots of global density, orientation and alignment of the swarm as a function of time
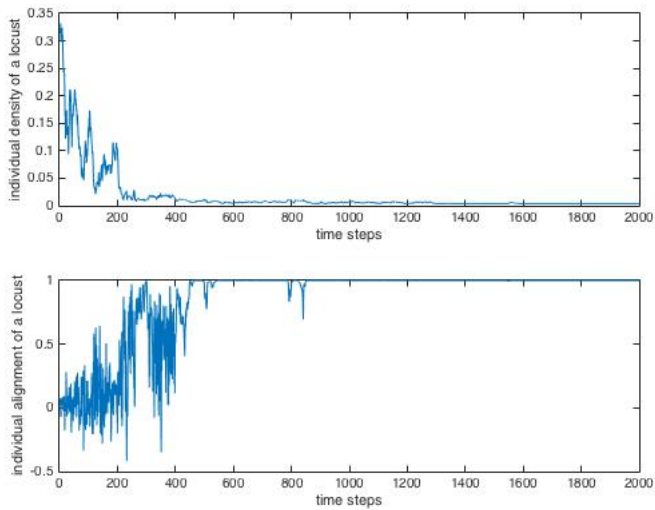
Figure 5.5   Example 1: Local alignment of an individual locust as a function of time
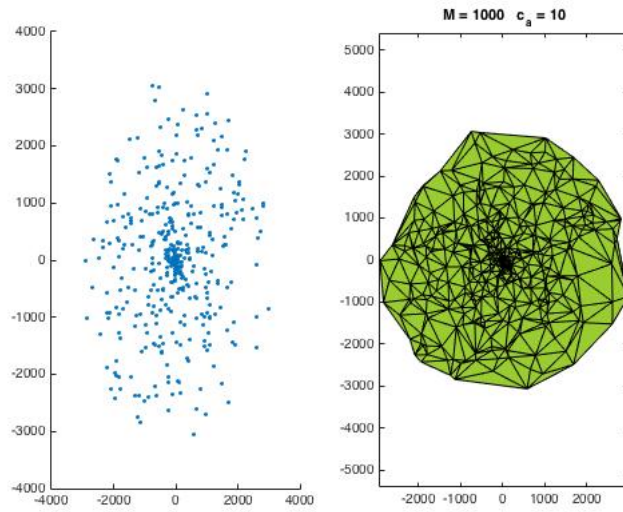
Figure 5.6   Example 2: Plots of the point cloud at the final time step

locusts is $M = 1000$, the initial density was set to 1, the time step was $\Delta = 0.5$, and the results are shown for 4000 time steps.
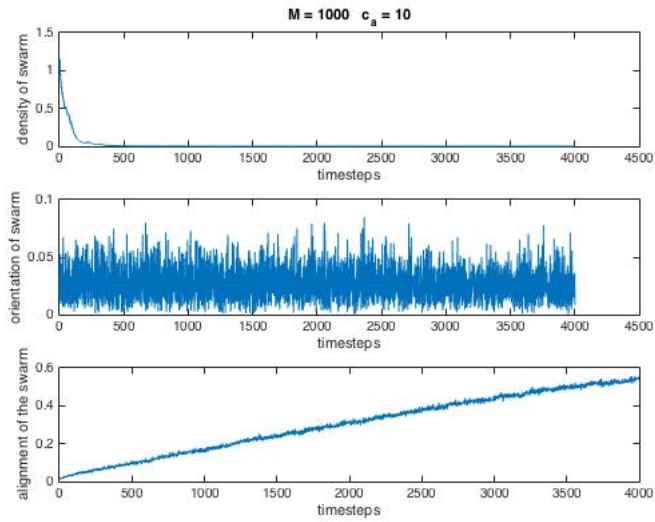
Example 2   29

Figure 5.7   Example 2: Plots of global density and alignment of the swarm as a function of time
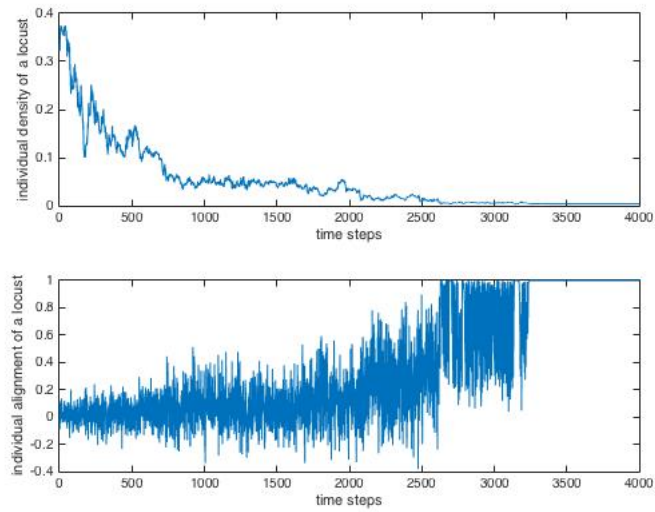
Figure 5.8   Example 2: Local alignment of an individual locust as a function of time
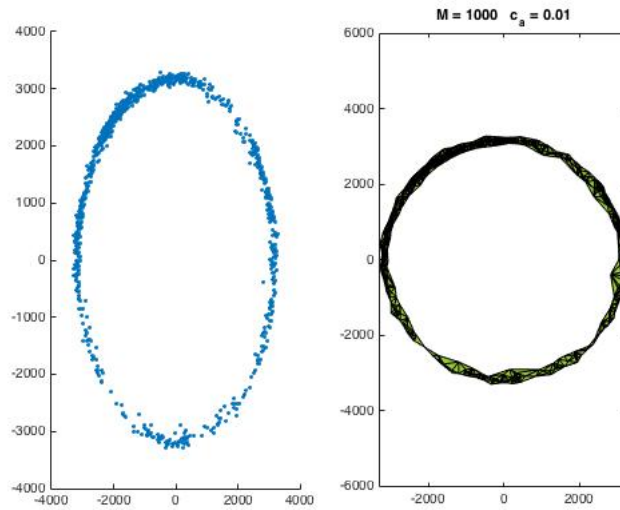
Figure 5.9 Example 3: Plots of the point cloud at the final time step

5.9 Example 3

In Figures 5.9-5.11, we show another example where we have set the alignment constant to be very small ($c_a = 0.01$). We set the total number of locusts to be $M = 1000$ and the time step to be $\Delta t = 1$. The other parameters are the same as Example 2. In this case, we see that the locusts seem to spread outwards as a ring.
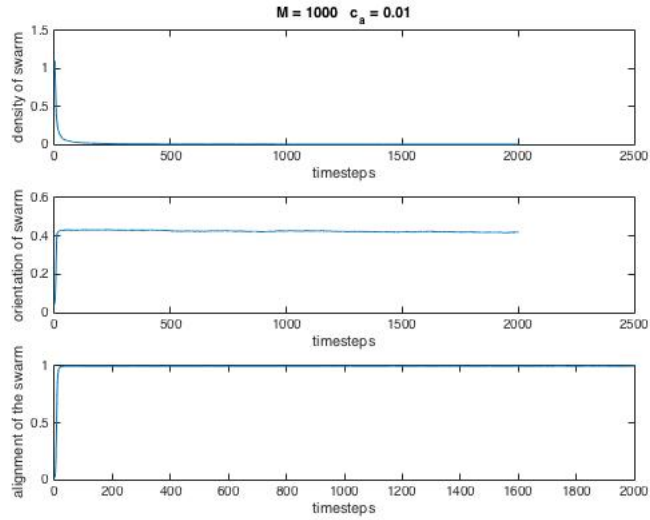
Example 3   **31**

Figure 5.10   Example 3: Plots of global density, orientation and alignment of the swarm as a function of time
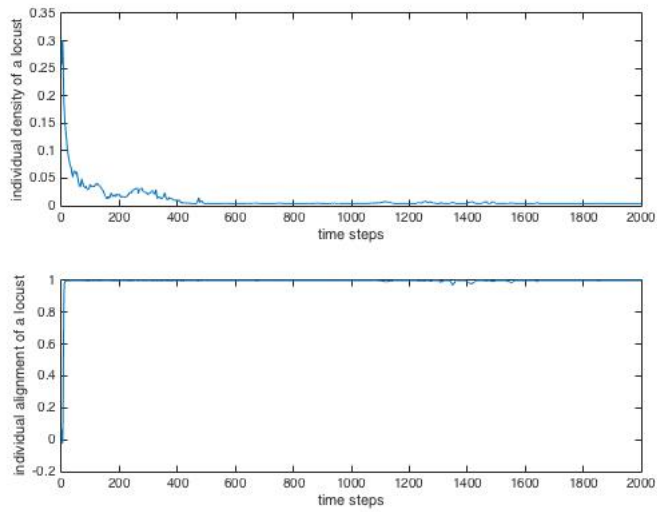
Figure 5.11   Example 3: Local alignment of an individual locust as a function of time

5.10   Clustering Algorithm For Identifying Fingering in the Swarm

Swarms in the biological world often exhibit a phenomenon known as 'fingering', where the swarm is initially clumped together, but eventually evolves into strands moving in different directions. This phenomenon can also be seen in our numerical simulations, given that the parameters are chosen appropriately. For instance, in Figure 7, we can see a clear sign of fingering. To identify fingering numerically, we define a metric in the 3-dimensional phase space (x, y, θ), where (x, y) is the location of an individual locust and θ is its current orientation. We say the two locusts are *connected* if their coordinates in the phase space satisfy

$$\sqrt{(x_1 - x_2)^2 + (y_1 - y_2)^2} \leq \varepsilon_x$$

and

$$|\theta_1 - \theta_2| \leq \varepsilon_\theta$$

where ε_x and ε_θ are constants. The idea is that two locusts are connected if both their physical location and their orientation are close enough. A simple choice for ε_x is just $\varepsilon_x = \ell_a$ (recall that this is the sensing distance for alignment). Choosing ε_θ is a bit more difficult. Recall that in continuous time we have

$$\frac{d\theta_i}{dt} = - \sum_{j=1, j\neq 1}^{n} c_a \left(1 - \frac{z_{ij}}{\ell_a}\right) \sin(\theta_i - \theta_j) + q\xi.$$

We claim that the variance of θ in this model is given by

$$\text{var}(\theta) = \frac{q^2}{2k}$$

where q is the width of the Gaussian noise and k is the linear restoring force given by

$$k = c_a \rho_{\text{loc}} \cdot 2\pi \int_0^{\ell_a} \left(1 - \frac{z}{\ell_a}\right) z \, dz.$$

Therefore, the standard deviation in θ is

$$\text{std}(\theta) = C \frac{q}{\ell_a \sqrt{c_a \rho_{\text{loc}}}}$$

10000 locusts after 1000 time steps

(a)

Centimeter
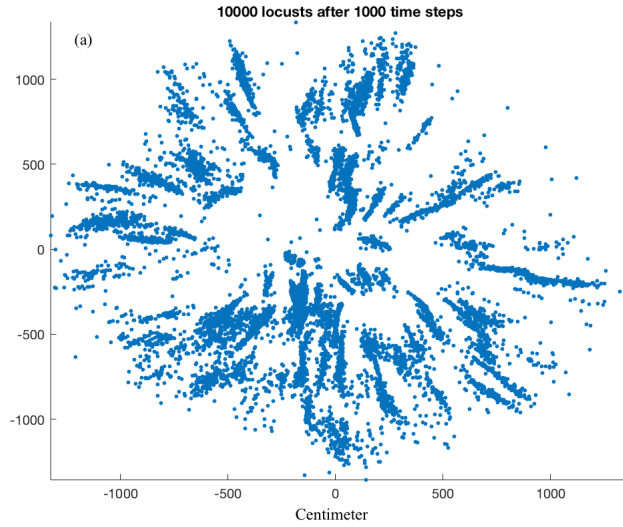
Figure 5.12   Fingering in a swarm of 10000 locusts

where C is some constant. Now we choose ε_θ as a constant multiple of the standard deviation. Thus

$$\varepsilon_\theta = C_0 \frac{q}{\ell_a \sqrt{c_a \rho_{\text{loc}}}}$$

where C_0 is simply a scaling constant.

Using our definition of connectedness, we can build an adjacency matrix $A = (a_{ij})$, of size M by M, where $a_{ij} = 1$ if the i-th and j-th locusts are connected, and $a_{ij} = 0$ otherwise. Using this adjacency matrix, we can construct a graph and identify its connected components. For swarms that exhibit fingering, we would expect to see a number of components with a significant number of locusts, corresponding to the strands of locusts traveling in different direction. This gives us a method for characterizing fingering behavior quantitatively. Figure 5.12 shows the one resulting configuration for a swarm of 10000 locusts. Figure 5.13 shows the result of our clustering algorithm of the swarm, with different colors corresponding to different fingers.
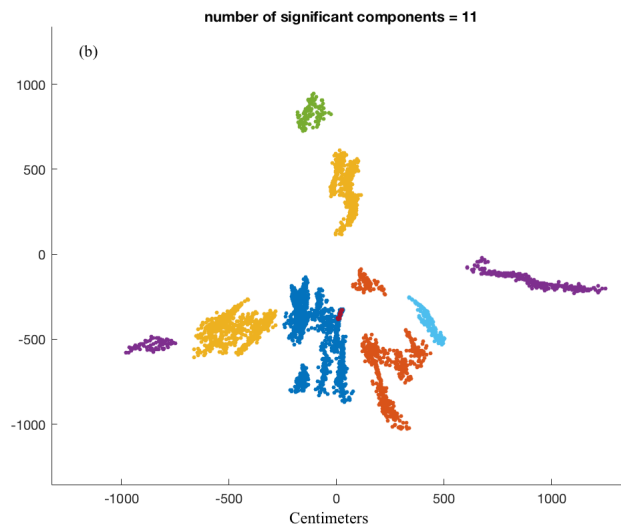
Figure 5.13   Identification of components in a swarm of 10000 locusts

Chapter 6

New Model for Periodic Domains

In this chapter, we will develop a new model for the movement of locusts on periodic domains. The equations of motion governing the state variables x, u and s are similar to the previous model. However, we also introduce a new mechanism by which a single isolated locust can acquire the tendency to move towards a marching band. Consider the situation that a single locust wanders off from a highly aligned marching band of locusts. In the old model, the single locust will still try to align with the marching band (via the θ equation). However, the locust will fail to move back into the marching band. In the new model, we address this issue by adding a new equation.

6.1 Equations of Motion On Periodic Domain

Recall that in Chapter 3, we introduced a model for the motion of locusts on an infinite 2-dimensional plane. The equations of motion were given by

$$\frac{dx_i}{dt} = v_0 s_i \hat{u}_i \qquad \text{(update the position vector)}$$

$$\frac{d\theta_i}{dt} = -\sum_{j=1}^{n} g(z_{ij}) \sin(\theta_i - \theta_j) + W \qquad \text{(update the orientation)}.$$

Here $\hat{u}_i = (\cos\theta_i, \sin\theta_i)$, $z_{ij} = \|x_i - x_j\|$, W is a Gaussian noise term in the angle, and $g(z_{ij})$ is a weighting function that decreases with distance. At each time step, the state variable s_i has a probability of transitioning from

stop to go $(0 \to 1)$ and vice versa. In our new model, we introduce a third equation given by

$$\frac{d\theta_i}{dt} = -\sum_{j=1}^{n} f(z_{ij}) \sin(\theta_i - \psi_j). \tag{6.1}$$

Here ψ_j is the angle between θ_i and the vector $\vec{z_{ij}}$, and $f(z_{ij})$ is another weighting function.

To restrict the locusts to a rectangular domain of size m by n, we simply take x and y component of the position vector $\vec{x_i}$ and mod out m and n, respectively. The distance between two locusts then, is computed on the periodic domain.

6.2 Particle-in-Cell Method for Periodic Domain

For the model in Chapter 3, we used the Particle-In-Cell method that was described in Ryan Jones' Senior Thesis (Jones, 2016). In the new periodic domain, this method is modified accordingly. In the original method, the whole domain was divided into square cells, and each cell had 8 neighboring cells. When consider the interaction between locusts, we only consider the current cell that the locust is in and its neighboring cells. For the periodic domain, we must be careful at the boundary of the domain, because the neighboring of the cells on the boundary is different from that of an infinite domain. In the implementation of the numerical method, the boundary cells are considered separately from the interior cells, and the distance functions are also specified.

6.3 Higher-order Stepping Method

In Chapter 3, we used Euler's method to update the state variables in our equations of motion. On the periodic domain, we used a higher-order stepping method known as the *modified Euler's method*. This method is described as follows. Suppose that we want to solve a differential equation of the form $y' = f(t, y)$. Our goal is to construct $w_1, w_2, \ldots, w_n$, where w_i is the approximation to $y(t_i)$. We use the following updates:

$$w_0 = \alpha, \tag{6.2}$$

$$w_{i+1} = w_i + \frac{h}{2}[f(t_i, w_i) + f(t_{i+1}, w_i + hf(t_i, w_i))] \tag{6.3}$$
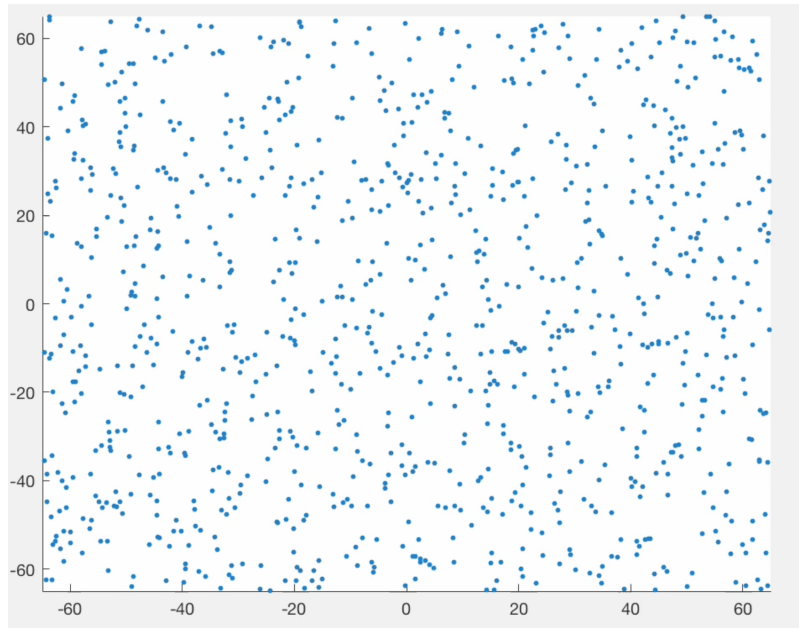
Figure 6.1   Initial state of 1000 locusts on the periodic domain

where α is the initial value and h is the step size. For our problem, y is the vector of state variables.

6.4   Results on the Periodic Domain

Figures 6.1 and 6.2 show the results of a simulation of 1000 locusts. We see that the locusts start with random initial conditions, but later evolve to reach a stable steady state with a clear pattern. This is a very interesting phenomenon, and in our future work we wish to construct a PDE that can characterize this steady state solution.
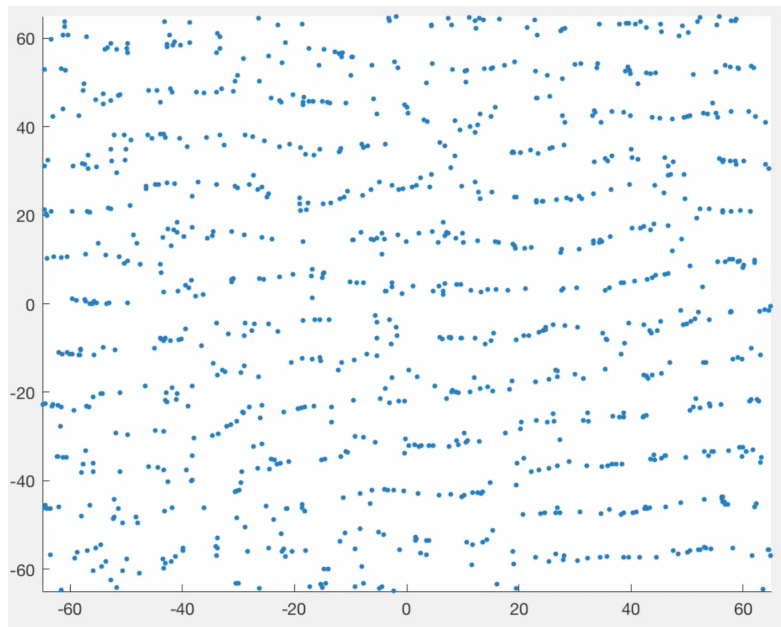
Figure 6.2   Pattern formation on the periodic domain

Chapter 7

Continuous Model

7.1   Introduction

In the first six chapters, we have derived an ODE model for modeling the behavior of locust hopper bands. In this chapter we want to build a PDE model that is continuous in both space and time.

   Our model is derived on the periodic rectangular domain $\Omega \in \mathbb{R}^2$. We have four state variables S, M, θ_s and θ_m, where S is the density of the locusts at rest, M is the density of the locust in motion, θ_s is the current orientation of the stationary locusts and θ_m is the current orientation of the moving locusts. Note that all state variables are functions of position $\vec{x}$ and time t.

   Roughly speaking, our PDE model is based on the same biological mechanics as the ODE model. The equations for S and M govern the transition of the locusts between stationary and moving states, and the equations for θ_m and θ_s govern the change of orientation in the locust swarm.

7.2   Transition Between Stationary and Moving

We define β_m and β_s to be the block score for moving and stationary locusts, respectively. The total density is

$$\rho(\vec{x}, t) = S(\vec{x}, t) + M(\vec{x}, t).$$

The transition between stationary and moving is governed by

$$\frac{\partial S}{\partial t} = -k_1(\rho)S + k_2(\rho)M \tag{7.1}$$

$$\frac{\partial M}{\partial t} + \nabla \cdot (\vec{u}M) = k_1(\rho)S - k_2(\rho)M \tag{7.2}$$

The parameters k_1 and k_2 are functions of ρ. Recall that in the previous ODE model, we had $k_1 = \kappa_1 e^{-a_1\beta}$ and $k_2 = \kappa_2 e^{a_2\beta}$, where β was the block score, given by

$$\beta = \sum_{j=1, j\neq i} \left(1 - \frac{z_{ij}}{\ell_b}\right)\cos\phi_{ij}.$$

Analogously, in the continuum model, we can write

$$\beta_m = \int_{\mathbb{R}^2} f(|\vec{y} - \vec{x}|)\cos(\theta_m(\vec{x}) - \arg(\vec{y} - \vec{x}))\rho(\vec{y})\,d\vec{y},$$

$$\beta_s = \int_{\mathbb{R}^2} f(|\vec{y} - \vec{x}|)\cos(\theta_s(\vec{x}) - \arg(\vec{y} - \vec{x}))\rho(\vec{y})\,d\vec{y},$$

where

$$f(z) = \left(1 - \frac{z_{ij}}{\ell_b}\right)$$

and $\arg\vec{y}$ is the phase of the position vector $\vec{y}$. It follows that $k_1 = \kappa_1 e^{-a_1\beta_s}$ and $k_2 = \kappa_2 e^{a_2\beta_m}$.

7.3   Evolution of orientation

The equations for θ_m and θ_s are similar to the θ equation in the discrete model, which was based on the Kuramoto model for synchronization. Both moving and stationary locusts tries to align themselves with nearby locusts, and the strength of the alignment is scaled by the density of the surrounding locusts. For the θ_m equation, we have the convection term $\nabla \cdot (\vec{u}\theta_m)$, which is based on the continuum equation in fluid dynamics.

$$\frac{d\theta_s}{dt} = -\int_{\mathbb{R}^2} g(|\vec{y} - \vec{x}|)\left[S(\vec{y})\sin(\theta_s(\vec{x}) - \theta_s(\vec{y})) + M(\vec{y})\sin(\theta_s(\vec{x}) - \theta_m(\vec{y}))\right]\,d\vec{y}$$

$$\tag{7.3}$$

$$\frac{d\theta_m}{dt} + \nabla \cdot (\vec{u}\theta_m) = -\int_{\mathbb{R}^2} g(|\vec{y} - \vec{x}|)\left[S(\vec{y})\sin(\theta_m(\vec{x}) - \theta_s(\vec{y})) + M(\vec{y})\sin(\theta_m(\vec{x}) - \theta_m(\vec{y}))\right])\,d\vec{y}$$

$$\tag{7.4}$$

where $g(z)$ is the weighting function given by

$$g(z) = \left(1 - \frac{z_{ij}}{\ell_\theta}\right).$$

7.4 Stationary Solutions

To find the stationary solutions, we set the time derivatives of the four state variables to be 0. For the θ equations, one obvious solution is attained by setting θ_m and θ_s to be constant. Also, we can set $M(\vec{x}, t)$ and $S(\vec{x}, t)$ to be constants as well, so this will give us

$$\frac{M(\vec{x}, t)}{S(\vec{x}, t)} = \frac{k_2(\rho)}{k_1(\rho)}.$$

Since both M and S are constant, ρ is also a constant, so k_1, k_2 are fixed, which means that the ratio between M and S are also fixed.

Suppose that we make the assumption that all the variables $S, M, \beta_s, \beta_m, \theta_s$ and θ_m are homogeneous in the horizontal direction (in other words, they are only functions of y, the vertical position, and t), then the equations can be written in a simpler form. First, let us consider the block scores β_m and β_s at a point $(x_0, y_0) \in \mathbb{R}^2$. Suppose that the the sensing radius is R, then the block score is in fact computed through an integral over a circle of radius R centered at (x_0, y_0). We have

$$\beta_m = \int_{\eta=-R}^{\eta=R} \int_{-\sqrt{R^2-\eta^2}}^{\sqrt{R^2-\eta^2}} f(\sqrt{x^2 + \eta^2}) \cdot \cos(\theta_m(y_0) - \tan^{-1}(\frac{\eta}{x}) \cdot \rho(y_0 + \eta) \, dx.$$

$$\beta_s = \int_{\eta=-R}^{\eta=R} \int_{-\sqrt{R^2-\eta^2}}^{\sqrt{R^2-\eta^2}} f(\sqrt{x^2 + \eta^2}) \cdot \cos(\theta_s(y_0) - \tan^{-1}(\frac{\eta}{x}) \cdot \rho(y_0 + \eta) \, dx.$$

Using the explicit form for f, we can write the rewrite the integral as

$$\beta_m = \sin(\theta_m(y_0)) \int_{\xi=-1}^{1} \rho(y_0 + \xi R)\xi h(\xi) \, d\xi,$$

$$\beta_s = \sin(\theta_s(y_0)) \int_{\xi=-1}^{1} \rho(y_0 + \xi R)\xi h(\xi) \, d\xi,$$

where

$$h(\xi) = \ln\left[\frac{1 + \sqrt{1 - \xi^2}}{1 - \sqrt{1 - \xi^2}}\right] - 2\sqrt{1 - \xi^2}.$$

The equations for θ_s can also be writen as

$$\frac{d\theta_s}{dt} = I_s + I_m,$$

where

$$I_s = -\int_{\eta=-R}^{\eta=R}\int_{-\sqrt{R^2-\eta^2}}^{\sqrt{R^2-\eta^2}} g(\sqrt{x^2+\eta^2}) \cdot \sin(\theta_s(y_0) - \theta_s(y_0+\eta)) \cdot S(y_0+\eta)\,dx,$$

$$I_m = -\int_{\eta=-R}^{\eta=R}\int_{-\sqrt{R^2-\eta^2}}^{\sqrt{R^2-\eta^2}} g(\sqrt{x^2+\eta^2}) \cdot \sin(\theta_s(y_0) - \theta_M(y_0+\eta)) \cdot M(y_0+\eta)\,dx.$$

We can define

$$K(\eta) = \int_{-\sqrt{R^2-\eta^2}}^{\sqrt{R^2-\eta^2}} g(\sqrt{x^2+\eta^2})\,dx.$$

If we let

$$g(x) = 1 - \frac{x}{R},$$

then we have

$$K(\eta) = \int_{-\sqrt{R^2-\eta^2}}^{\sqrt{R^2-\eta^2}}(1 - \frac{\sqrt{x^2+\eta^2}}{R})\,dx.$$

The equations for θ_m are exactly the same except that we replace $\theta_s(y_0+\eta)$ with $\theta_m(y_0+\eta)$. The function $K(\eta)$ can be integrated to yield the closed form

$$K(\eta) = \frac{-\eta^2\ln(\sqrt{R^2-\eta^2}+R) + \eta^2\ln(-\sqrt{R^2-\eta^2}+R) + 2\sqrt{R^2-\eta^2}R}{2R}.$$

We can rewrite $K(\eta)$ as a new function $L(\xi)$, where $\xi = \eta/R$. Then the kernel of integration $K(\eta)$ becomes

$$L(\xi) = \frac{1}{2R}\left(\xi^2\ln\left(\frac{1-\sqrt{1-\xi^2}}{1+\sqrt{1-\xi^2}}\right) + 2\sqrt{1-\xi^2}\right).$$

Therefore, we can rewrite the the integrals I_s and I_m as

$$I_s = -\int_{\xi=-1}^{\xi=1} L(\xi)\sin(\theta_s(y_0) - \theta_s(y_0+R\xi)) \cdot S(y_0+R\xi)\,d\xi$$

$$I_m = - \int_{\xi=-1}^{\xi=1} L(\xi) \sin(\theta_s(y_0) - \theta_m(y_0 + R\xi)) \cdot M(y_0 + R\xi) \, d\xi.$$

For the θ_m equation, we can similarly define I'_s and I'_m to be

$$I'_s = - \int_{\xi=-1}^{\xi=1} L(\xi) \sin(\theta_m(y_0) - \theta_s(y_0 + R\xi)) \cdot S(y_0 + R\xi) \, d\xi$$

$$I'_m = - \int_{\xi=-1}^{\xi=1} L(\xi) \sin(\theta_m(y_0) - \theta_m(y_0 + R\xi)) \cdot M(y_0 + R\xi) \, d\xi.$$

Therefore, the equation simply becomes

$$\frac{\partial \theta_m}{\partial t} = I'_s + I'_m.$$

7.4.1   Linearization of PDEs

We want to linearize the PDEs that we obtained from the previous section, which can be written as only equations involving the two variables y and t.

$$\frac{\partial S}{\partial t} = -\kappa_1 \exp(-a_1 \beta_s) S(y, t) + \kappa_2 \exp(a_2 \beta_m) M(y, t) \tag{7.5}$$

$$\frac{\partial M}{\partial t} = -v_0 \frac{\partial}{\partial y} \left(\sin(\theta_m) \cdot M(y, t) \right) + \kappa_1 \exp(-a_1 \beta_s) S(y, t) - \kappa_2 \exp(a_2 \beta_m) M(y, t) \tag{7.6}$$

$$\frac{\partial \theta_s}{\partial t} = I_s + I_m \tag{7.7}$$

$$\frac{\partial \theta_m}{\partial t} = -v_0 \frac{\partial}{\partial y} \left(\sin(\theta_m) \cdot \theta_m(y, t) \right) + I'_s + I'_m. \tag{7.8}$$

Suppose that $\overline{S}, \overline{M}, \overline{\theta_s}, \overline{\theta_m}$ are the steady state solutions to the systems of PDEs. Notice that we have $\overline{\theta_s} = \overline{\theta_m} = 0$, thus we can perturb the steady state solutions and write

$$\begin{bmatrix} S \\ M \\ \theta_s \\ \theta_m \end{bmatrix} = \begin{bmatrix} \overline{S} \\ \overline{M} \\ 0 \\ 0 \end{bmatrix} + \varepsilon \begin{bmatrix} \hat{S} \\ \hat{M} \\ \hat{\theta}_s \\ \hat{\theta}_m \end{bmatrix} \cdot \exp\left(i\mu y + \lambda t \right),$$

where $\hat{S}, \hat{M}, \hat{\theta}_s$ and $\hat{\theta}_m$ are just constants. Plugging this back in to the equation, we get

$$\lambda \hat{S} = -\kappa_1 \hat{S} + \kappa_2 \hat{M}.$$

$$\lambda \hat{M} = -v_0 \overline{M}[i\mu]\hat{\theta}_m + \kappa_1 \hat{S} - \kappa_2 \hat{M}.$$

After the perturbation, we also have

$$I_s = -\sin(\theta_s(y)) \int_{\xi=-1}^{\xi=1} \cos(\theta_s(y_0 + R\xi))L(\xi)S(y_0 + R\xi)d\xi$$

$$+ \cos(\theta_s(y)) \int_{\xi=-1}^{\xi=1} \sin(\theta_s(y_0 + R\xi))L(\xi)S(y_0 + R\xi)d\xi$$

$$\approx -e^{i\mu y + \lambda t}\hat{\theta}_s \overline{S} \int_{-1}^{1} L(\xi)d\xi - \overline{S}\int_{\xi=-1}^{\xi=1} \theta_s(y + R\xi)L(\xi)d\xi$$

$$\approx -e^{i\mu y + \lambda t}\hat{\theta}_s \overline{S} \left(\int_{-1}^{1} L(\xi)d\xi - \int_{\xi=-1}^{1} e^{i\mu R\xi}L(\xi)d\xi \right)$$

The results and similar for I_m, where we have

$$I_m = -\sin(\theta_s(y)) \int_{\xi=-1}^{\xi=1} \cos(\theta_m(y_0 + R\xi))L(\xi)M(y_0 + R\xi)d\xi$$

$$+ \cos(\theta_s(y)) \int_{\xi=-1}^{\xi=1} \sin(\theta_m(y_0 + R\xi))L(\xi)M(y_0 + R\xi)d\xi$$

$$\approx -e^{i\mu y + \lambda t}\hat{\theta}_s \overline{M} \int_{-1}^{1} L(\xi)d\xi - \overline{M}\int_{\xi=-1}^{\xi=1} \theta_m(y + R\xi)L(\xi)d\xi$$

$$\approx -e^{i\mu y + \lambda t}\overline{M} \left(\hat{\theta}_s \int_{-1}^{1} L(\xi)d\xi - \hat{\theta}_m \int_{\xi=-1}^{1} e^{i\mu R\xi}L(\xi)d\xi \right)$$

Similarly, we have

$$I'_s = -e^{i\mu y + \lambda t} \left(\hat{\theta}_m \overline{S} \int_{-1}^{1} L(\xi)d\xi - \hat{\theta}_s \overline{S} \int_{\xi=-1}^{1} e^{i\mu R\xi}L(\xi)d\xi \right)$$

$$I'_m = -e^{i\mu y + \lambda t}\hat{\theta}_m \overline{M} \left(\int_{-1}^{1} L(\xi)d\xi - \int_{\xi=-1}^{1} e^{i\mu R\xi}L(\xi)d\xi \right).$$

It follows that after the perturbation, the third equation becomes

$$\lambda \hat{\theta}_s = -\left(\int_{-1}^{1} L(\xi)d\xi \right)(\overline{S}\hat{\theta}_s + \overline{M}\hat{\theta}_s) + \left[\int_{\xi=-1}^{1} e^{i\mu R\xi}L(\xi)d\xi \right](\hat{\theta}_s\overline{S} + \hat{\theta}_m\overline{M}).$$

The linearization of the fourth equation is similar, and we get

$$\lambda \hat{\theta}_m = -\left(\int_{-1}^{1} L(\xi)d\xi \right)(\overline{S}\hat{\theta}_m + \overline{M}\hat{\theta}_m) + \left[\int_{\xi=-1}^{1} e^{i\mu R\xi}L(\xi)d\xi \right](\hat{\theta}_s\overline{S} + \hat{\theta}_m\overline{M}).$$

We can define

$$w = \int_{-1}^{1} L(\xi)d\xi$$

and the function

$$C(\mu R) = \int_{\xi=-1}^{1} e^{i\mu R \xi} L(\xi)d\xi.$$

Thus we can write out the whole linearized system as

$$\lambda \begin{bmatrix} \hat{S} \\ \hat{M} \\ \hat{\theta}_s \\ \hat{\theta}_m \end{bmatrix} = \mathcal{M}(\mu, \mathcal{R}) \begin{bmatrix} \hat{S} \\ \hat{M} \\ \hat{\theta}_s \\ \hat{\theta}_m \end{bmatrix},$$

where

$$\mathcal{M}(\mu, \mathcal{R}) = \begin{bmatrix} -\kappa_1 & \kappa_2 & 0 & 0 \\ \kappa_1 & -\kappa_2 & 0 & -v_0\overline{M}[i\mu] \\ 0 & 0 & -w(\overline{S}+\overline{M})+C(\mu R)\overline{S} & C(\mu R)\overline{M} \\ 0 & 0 & C(\mu R)\overline{S} & -w(\overline{S}+\overline{M})+C(\mu R)\overline{M} \end{bmatrix}.$$

Now notice that $\overline{S} + \overline{M} = \overline{\rho}$, then we can define a few new variables to simplify computations. Let $\alpha = \mu R$, $S = \overline{S}/\overline{\rho}$, $m = \overline{M}/\overline{\rho}$, and we also define

$$d = \frac{C(\alpha)}{C(0)} \qquad \tilde{\lambda} = \frac{\lambda}{C(0)\rho}.$$

Now we denote that upper left block matrix in $\mathcal{M}(\alpha)$ by A and the lower right block matrix by B. Then we can write

$$B - \lambda I = C(0)\overline{\rho} \cdot [\tilde{A} - \tilde{\lambda}I],$$

where

$$[\tilde{A} - \tilde{\lambda}I] = \begin{bmatrix} -1 - \tilde{\lambda} + Sd(\alpha) & d(\alpha)m \\ d(\alpha)S & -1 - \tilde{\lambda} + d(\alpha)m \end{bmatrix}.$$

By setting

$$\det([\tilde{A} - \tilde{\lambda}I]) = 0,$$

we find that the eigenvalues of B are simply

$$\tilde{\lambda}_1 = -1, \qquad \tilde{\lambda}_2 = d(\alpha) - 1.$$

It is easy to see that the eigenvalues for A are just

$$\lambda_1 = -(k_1 + k_2), \qquad \lambda_2 = 0.$$

The eigenvalues provide us with information about the stability of the stationary solution. By explicitly computing $d(\alpha)$, we see that $d(\alpha) \leq 1$, so both $\tilde{\lambda}_1$ and $\tilde{\lambda}_2$ are less than 0. Therefore, in total we have three negative eigenvalues and one that is equal to 0.

Chapter 8

Conclusions and Future Work

Presented here is a summary of what we have done over the duration of this thesis. We have completed a literature review of biological literature of locust swarms and summarized the information that are relevant to our model. We have developed both an agent-based model the behavior of locust swarms. The equations of motion were motivated by the Kuramoto model for synchronization and the parameters in the model was estimated through the biological literature. To deal with a large number of locusts, we also used the particle in cell method that was first developed by Ryan Jones in his senior thesis (Jones 2016). As a result, we were able to observe fingering on the infinite domain, which is a key feature of the agent-based model. We also developed various metrics, such as the global and local alignment scores, for characterizing the geometry of the swarms and determining if the equations have reached equilibrium. In the Fall semester, we changed from an infinite domain to a rectangular periodic domain. We also added an attraction term between the locusts. To make the numerical method for solving the equations more stable, we used a higher-order stepping method. Consequently, we observed striped patterns on the periodic domain. During the Spring semester, we started developing a PDE model that treats the locust swarms as a density function on a periodic domain. To analyze the PDEs, we first considered a solution that is homogeneous in the horizontal direction, so that all the variables only depend on the vertical position and time. As a result, we were able to linearize the PDEs near a stationary solution. However, the results of linearization do not quite match observations of the agent-based model on the periodic domain. One possible issue is that we have not yet included the attraction term, and therefore a key component is still missing. Further work can include deriving additional PDEs for modeling attraction

between locusts. Another might be to include environmental cues such as food sources into our model.

Bibliography

Gil Ariel, Yotam Ophir, Sagi Levi, Eshel Ben-Jacob, and Amir Ayali. Individual pause-and-go motion is instrumental to the formation and maintenance of swarms of marching locust nymphs. *PloS one*, 9(7):e101636, 2014.

Sepideh Bazazi, Jerome Buhl, Joseph J Hale, Michael L Anstey, Gregory A Sword, Stephen J Simpson, and Iain D Couzin. Collective motion and cannibalism in locust migratory bands. *Current Biology*, 18(10):735–739, 2008.

Sepideh Bazazi, Frederic Bartumeus, Joseph J Hale, and Iain D Couzin. Intermittent motion in desert locusts: behavioural complexity in simple environments. *PLoS Comput Biol*, 8(5):e1002498, 2012.

Jerome Buhl, David JT Sumpter, Iain D Couzin, Joe J Hale, Emma Despland, ER Miller, and Steve J Simpson. From disorder to order in marching locusts. *Science*, 312(5778):1402–1406, 2006.

Jerome Buhl, Gregory A Sword, Fiona J Clissold, and Stephen J Simpson. Group structure in locust migratory bands. *Behavioral ecology and sociobiology*, 65(2):265–273, 2011.

Louise Dyson, Christian A Yates, Jerome Buhl, and Alan J McKane. Onset of collective motion in locusts is captured by a minimal model. *Physical Review E*, 92(5):052708, 2015.

Ryan Jones. Hopper bands: Locust aggregation. *Harvey Mudd College Senior Thesis*.

Lee A. Segel and Leah Edelstein-Keshet. *A Primer in Mathematical Models in Biology*, volume 129. SIAM, 2013.

Steven H Strogatz. From kuramoto to crawford: exploring the onset of synchronization in populations of coupled oscillators. *Physica D: Nonlinear Phenomena*, 143(1):1–20, 2000.

PM Symmons and K Cressman. Desert locust guidelines: biology and behaviour. *Rome: Food and Agriculture organization (FAO) of the United Nations*, 2001.

Christian A Yates, Radek Erban, Carlos Escudero, Iain D Couzin, Jerome Buhl, Ioannis G Kevrekidis, Philip K Maini, and David JT Sumpter. Inherent noise can facilitate coherence in collective swarm motion. *Proceedings of the National Academy of Sciences*, 106(14):5464–5469, 2009.